### Title

Iron Speciation in Respirable Particulate Matter and Implications for Human Health




### Journal

Environmental Science and Technology, 56(11)

### ISSN

0013-936X



### Authors

O'Day, Peggy A

Pattammattel, Ajith

Aronstein, Paul

et al.



### Publication Date

2022-06-07

### DOI

10.1021/acs.est.1c06962

Peer reviewed

Environmental Science & Technology

pubs.acs.org/est

Article

# Iron Speciation in Respirable Particulate Matter and Implications for Human Health

Peggy A. O'Day,* Ajith Pattammattel, Paul Aronstein, Valerie J. Leppert, and Henry Jay Forman

Cite This: *Environ. Sci. Technol.* 2022, 56, 7006−7016

Read Online

ACCESS | Metrics & More | Article Recommendations | Supporting Information

**ABSTRACT:** Particulate matter (PM) air pollution poses a major global health risk, but the role of iron (Fe) is not clearly defined because chemistry at the particle−cell interface is often not considered. Detailed spectromicroscopy characterizations of $PM_{2.5}$ samples from the San Joaquin Valley, CA identified major Fe-bearing components and estimated their relative proportions. Iron in ambient $PM_{2.5}$ was present in spatially and temporally variable mixtures, mostly as Fe(III) oxides and phyllosilicates, but with significant fractions of metallic iron (Fe(0)), Fe(II,III) oxide, and Fe(III) bonded to organic carbon. Fe(0) was present as aggregated, nm-sized particles that comprised up to ∼30% of the Fe spectral fraction. Mixtures reflect anthropogenic and geogenic particles subjected to environmental weathering, but reduced Fe in PM originates from anthropogenic sources, likely as abrasion products. Possible mechanistic pathways involving Fe(0) particles and mixtures of Fe(II) and Fe(III) surface species may generate hydrogen peroxide and oxygen-centered radical species (hydroxyl, hydroperoxyl, or superoxide) in Fenton-type reactions. From a health perspective, PM mixtures with reduced and oxidized Fe will have a disproportionate effect in cellular response after inhalation because of their tendency to shuttle electrons and produce oxidants and electrophiles that induce inflammation and oxidative stress.

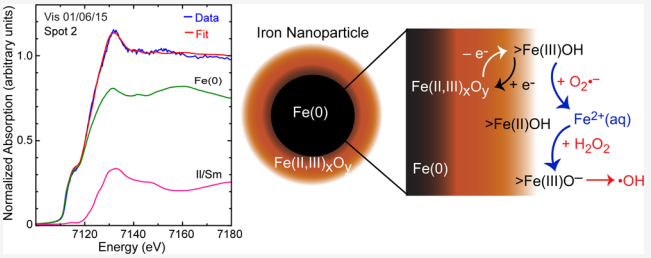


**KEYWORDS:** *$PM_{2.5}$, iron, X-ray absorption spectroscopy, electron energy loss spectroscopy, inflammation, oxidative stress, nanoparticles, Fenton reactions*

## INTRODUCTION

Particulate matter (PM) air pollution poses a major health risk that impacts over 90% of the world's population, especially in poor and developing nations.[1] Inhalation of PM, particularly in the size range of 2.5 $\mu$m ($PM_{2.5}$) or less, is associated with increased risks of cardiopulmonary diseases and stroke, and increased vulnerability to inflammation-associated pathologies such as respiratory diseases and lung cancers.[1−5] Exposure to fine-fraction PM is associated with an increased or exaggerated inflammatory response and a decreased capacity to adapt to oxidative stress with aging, potentially increasing vulnerability to inflammation-associated pathologies such as Alzheimer's disease (AD).[3,6,7] For example, a recent population-based cohort study showed that an increased risk of AD and dementia was correlated with long-term exposure to $PM_{2.5}$ in the Seattle region.[8] Causal links between PM air pollution and health outcomes, however, are lacking. Reaction of PM mixtures with cells can generate both electrophile and oxidant species that have markedly different effects upon cells. They may directly damage cellular constituents and induce pro-inflammatory cytokines, a potentially damaging biological response, but may also induce expression of antioxidant enzymes as an adaptive protective cell response.[9−13] In addition to electron transfer, nanometer-sized metal particles associated with anthropogenic emissions ($PM_{1.0}$ and $PM_{0.1}$) may be both more reactive and pose a greater health risk compared to larger size fractions.[14−16]

Airborne PM is a complex mixture of organic and inorganic constituents emitted from a variety of primary sources and subjected to different types and degrees of secondary reprocessing and environmental weathering. Although exhaust emissions composed of carbonaceous compounds dominate urban PM pollution, nonexhaust emissions are expected to constitute an increasingly higher fraction of respirable PM in urban areas and near roadways and transportation systems as combustion emissions decline due to regulatory controls.[17,18] Iron (Fe) is the most abundant transition metal element found in PM on average, generally followed by copper (Cu) at about 1−2 orders of magnitude lower concentration.[19,20] Urban nonexhaust emissions are dominated by anthropogenic sources of metal-bearing particles[21,22] and they have been linked to a range of adverse health outcomes.[23,24]

**Special Issue:** Urban Air Pollution and Human Health

**Received:** October 13, 2021
**Revised:** January 19, 2022
**Accepted:** February 8, 2022
**Published:** March 2, 2022

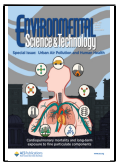

While size and element compositions are routinely measured in PM, few prior studies have examined in detail the chemical speciation of Fe, including element oxidation state(s), chemical form (i.e., crystalline phase, amorphous phase, minor substituent in a crystalline phase, or adsorbed species), and relative abundances of Fe-bearing constituents. In general, the contribution of nonexhaust emissions to PM is poorly quantified.[16] We recently reported Fe speciation, oxidation states, and relative abundance of Fe-bearing phases in $PM_{2.5}$ samples from two locations in urban Los Angeles (LA), CA, and reviewed previous studies characterizing Fe speciation in PM.[25] Prior studies reported a variety of Fe species and phases depending on the particle size fraction and method of interrogation, but most reported qualitative observations, with results that depended to some extent on the method(s) of characterization. Iron and other metal species in PM may be derived from both geogenic (Earth material) and anthropogenic sources. For some constituents, particularly common Fe-oxide and Fe-bearing phyllosilicate phases, distinguishing between geogenic and anthropogenic origins, and secondary alteration or reprocessing, is not always possible. Our study of LA $PM_{2.5}$ samples and review of potential sources suggested that the majority of Fe-bearing PM from this urban area was anthropogenic, primarily abrasion products from vehicle braking systems and engine emissions from combustion and/or wear.[25]

In this study, we combined bulk and spatially resolved spectroscopy and microscopy for a detailed interrogation of Fe speciation in $PM_{2.5}$ from two urban areas (~70 km apart) within the agricultural region of the southern San Joaquin Valley (SJV), CA collected on two consecutive weeks in winter and summer. This geographic area has exceeded annual $PM_{2.5}$ outdoor air pollution standards every year for the last two decades,[26] and suffers from high rates of asthma and respiratory and cardiovascular diseases.[27,28] We provide direct spectroscopic and microscopic evidence of the chemical forms of Fe and their host phases, and estimate relative proportions of Fe species in ambient $PM_{2.5}$ from bulk spectral analysis. These results are used to propose a mechanism of electron transfer at the surfaces of Fe-bearing particles in biological fluids that can generate transient radical and reactive species with known links to adverse health outcomes.

## MATERIALS AND METHODS

**$PM_{2.5}$ Sample Sites.** Filter samples for detailed spectromicroscopy characterization were obtained in June 2015 from the San Joaquin Valley Air Pollution Control District (SJVAPCD) from two monitoring sites, Fresno Garland (Gar) and Visalia (Vis), collected in January 2015 and May–June 2014 (Supporting Information (SI) Table S1 and Figure S1). Additional samples from two other stations, Fresno Hamilton (Ham) and Merced (Mer), collected in winter 2011–2012 (obtained in October 2013) were examined by bulk XAS and are included for comparison. Samples were collected by the standard EPA method for 24-h $PM_{2.5}$ continuous monitoring.[29] Total mass and bulk chemical analyses for carbon, inorganic species, and elements were provided by the SJVAPCD for Gar and Vis samples (SI Figures S2 and S3, Table S2). See SI for analytical details and results.

**X-ray Absorption Spectroscopy (XAS).** Bulk XANES and EXAFS spectra were collected at the Stanford Synchrotron Radiation Lightsource (SSRL) on wiggler beamline 4–1 using a Si(220) monochromator. Teflon filters as received were mounted onto Al-holders, sealed using sulfur-free tape, and held at liquid $N_2$ temperature for data collection. The monochromator was detuned by ~50% from maximum energy for rejection of high-order harmonic reflections, and beam size was 1 × 7 mm. Energy for the Fe K-edge was calibrated using the first inflection on the absorption edge of Fe metal foil, set at 7112.0 eV. X-ray fluorescence was collected using a Mn filter (Z-1) and soller slits placed between the sample and a solid state Ge detector (Canberra 32 element). Multiple spectra (to $k \sim 10-12$ Å$^{-1}$) were collected and averaged for each sample. XANES and EXAFS regions of the spectra were separated, and background subtraction and normalization were optimized for each region to closely match the normalization of the reference spectra used for fits. Pre-edge correction, postedge normalization, and linear combination (LC) fitting of the XANES and EXAFS were performed using ATHENA.[30] A previously published spectral library of known natural and synthetic Fe compounds were used for LC fits (SI Table S3).[25,31] Fits were performed without normalization; component fractions are reported as both raw fits and normalized to 100% for XANES and EXAFS separately (see SI for details of XAS fitting).

Spatially resolved $\mu$-XRF maps and $\mu$-XANES spectra were collected at SSRL beamline 2–3, using a ~ 2 $\mu$m size beam (Kirkpatrick-Baez mirror geometry). XRF maps ($\lambda_{ex}$ = 13050 eV, 25 s dwell time) were collected at room temperature using a Vortex 2X fluorescence detector. Samples were imaged directly on the Teflon filter and XANES spectra were collected on particles with sufficient Fe fluorescence counts. Data analysis was performed using SIXpack, X-ray microanalysis toolkit,[32] and ATHENA, similar to the methods for bulk spectra.

**Electron Microscopy and Electron Energy-Loss Spectroscopy (EELS).** Grids for transmission electron microscopy (TEM) were prepared from an aqueous dispersion of the PM prepared by sonication of the Teflon filter for 5 min in Milli-Q water and drop casted (2 $\mu$L) onto a 400-mesh holey carbon Cu grid (Ted Pella, Redding, CA). Grids were dried in a vacuum desiccator for at least 12 h before imaging. See SI for details of TEM and scanning transmission electron microscopy (STEM) data collection. STEM-electron energy-loss spectroscopy (EELS) data were collected at the Molecular Foundry (Lawrence Berkeley National Laboratory) using a Gatan imaging filter (GIF) on an F20 UT Tecnai microscope (200 kV) with a high-angle annular dark-field (HAADF) detector. Analyses of EELS data was performed using Gatan Digital Micrograph program (GMS3 Suite) provided by Gatan Inc. The $L_3/L_2$ ratio was estimated by the method described by van Aken and Liebscher;[33] application to $PM_{2.5}$ samples is described in detail in our prior publication.[25] Reference spectra were collected for stainless steel nanoparticles (Fe(0)), ilmenite ($FeTiO_3$), magnetite ($Fe_3O_4$), hematite ($\alpha$-$Fe_2O_3$), and ferrihydrite (amorphous $Fe(OH)_3$) (see SI for details of EELS data collection and analysis). The $L_3/L_2$ ratio estimated for these compounds was similar to previously reported values (±0.3) (SI Table S4).[34,35]

## RESULTS

**Mass and Chemical Composition.** Mass reconstructions based on compositional analysis of $PM_{2.5}$ samples at Gar and Vis sites showed a larger total mass by about 4–9 times measured in winter (January) compared with summer (May–June). The difference is due mostly to a much larger fraction associated with ammonium nitrate, which dominates $PM_{2.5}$


https://doi.org/10.1021/acs.est.1c06962
Environ. Sci. Technol. 2022, 56, 7006–7016

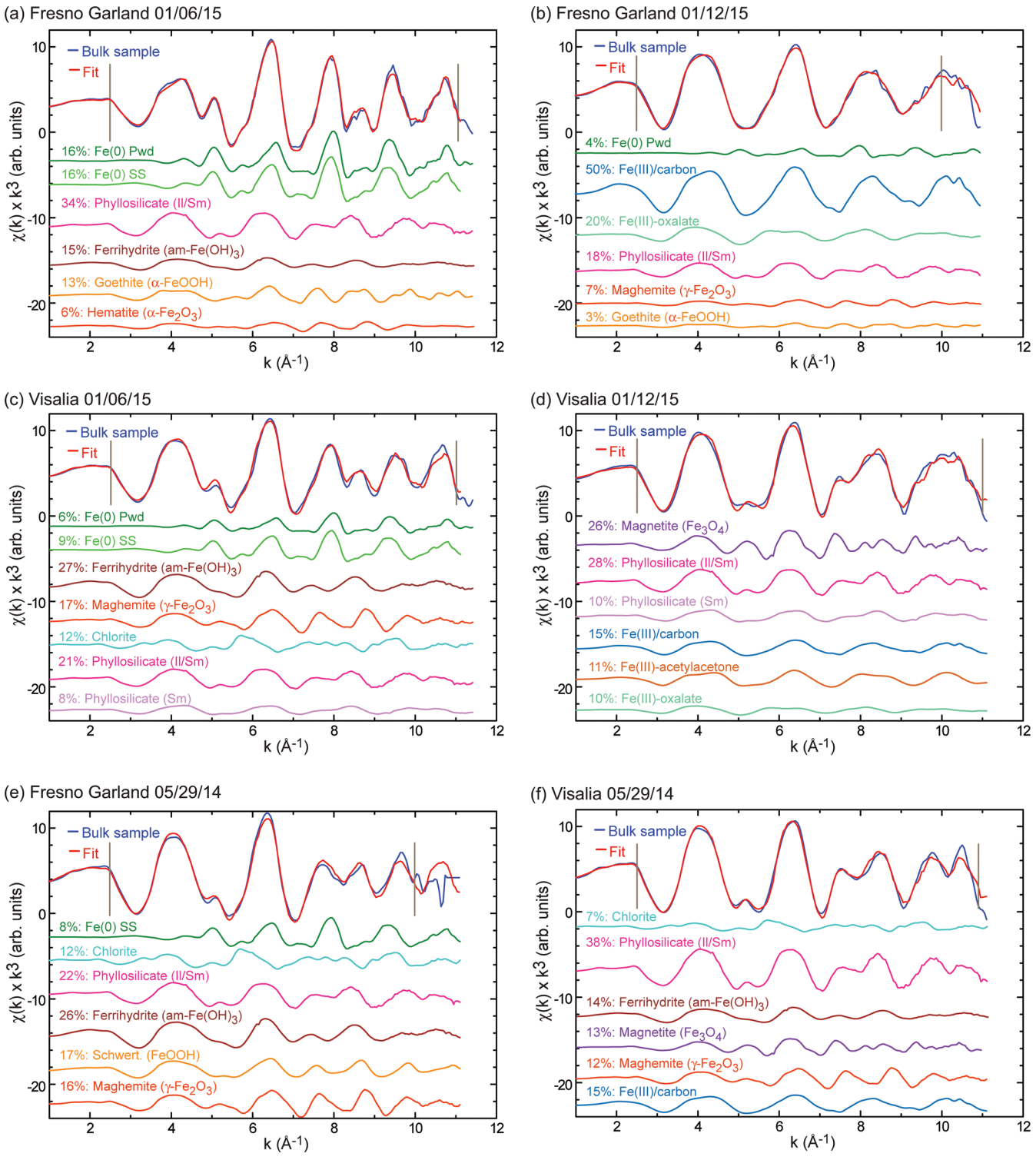


**Figure 1.** Bulk Fe K-edge EXAFS spectra of $PM_{2.5}$ samples collected on the same days: (a) Fresno Garland site in January and (b) same site collected 1 week later; (c) Visalia site in January and (c) same site collected 1 week later; (e) Fresno Garland and (f) Visalia in May. Data shown in blue, linear combination fits in red, and fractional component deconvolution of reference compound spectra shown below each fit. Vertical gray lines show the fitted region. See SI Tables S5 and S6 for numerical fit results.

mass in winter (SI Figure S2). Mass determined by the Federal Reference Method (FRM) gave a slightly different total mass but showed similar results as mass calculated by compositional reconstruction (see SI). Elemental carbon and organic matter fractions were higher overall in winter by about 3−4 times but constituted a similar mass fraction. The fraction classified as "geological", which includes a weighted fraction of the measured Fe concentration (SI Table S2), is about 2−3 times higher in summer than winter, and constitutes 16−25% of the total $PM_{2.5}$ mass, compared with ∼1% of total mass in winter. The remaining elements were generally less than 1 ug/$m^3$ (with the exception of Gar collected on 01/06/15 with 3.05



https://doi.org/10.1021/acs.est.1c06962
Environ. Sci. Technol. 2022, 56, 7006−7016

$\mu g/m^3$) and comprise ~1−6% of total mass. Among trace metals, Fe was most abundant (followed by Ca) and varied in concentration from 1.4 to 20 $\mu g/mg$ (SI Figure S3). Concentrations of Cu and Zn were ~1−2 orders of magnitude lower than Fe (Mn was below detection in Gar and Vis samples).

**X-ray Absorption Spectroscopy of $PM_{2.5}$.** *Bulk XANES and EXAFS.* Analysis of bulk normalized X-ray absorption spectra of $PM_{2.5}$ filter samples was done to identify and quantify relative proportions of the major Fe-bearing components. Comparison of $PM_{2.5}$ EXAFS spectra collected at Gar and Vis sites 1 week apart in winter and summer showed that Fe was present in multiple oxidation states and phases, and that proportions of these components varied spatially and temporally (Figure 1). Iron-bearing species were grouped by the following five major component groups, which each have distinctive spectral characteristics: metallic Fe(0); Fe(II) and Fe(II,III)-oxide phases; Fe(III)-oxide phases; phyllosilicate minerals (containing mostly Fe(III)); and Fe(III)-organic carbon associated. Within each group, multiple reference spectra were tested in fits to unknown spectra (SI Figures S4−S7; see SI for details and a complete list of reference compounds). A summary of the estimated normalized fractions from the best LC fits of reference spectra in separate XANES and EXAFS analysis is shown in Figure 2 (numerical fit results are given in SI Tables S5 and S6; additional XAS data are shown in SI Figures S8 and S9). Note that relative fractions refer to the five Fe-bearing component groups listed above and were not recalculated based on Fe mole fraction.

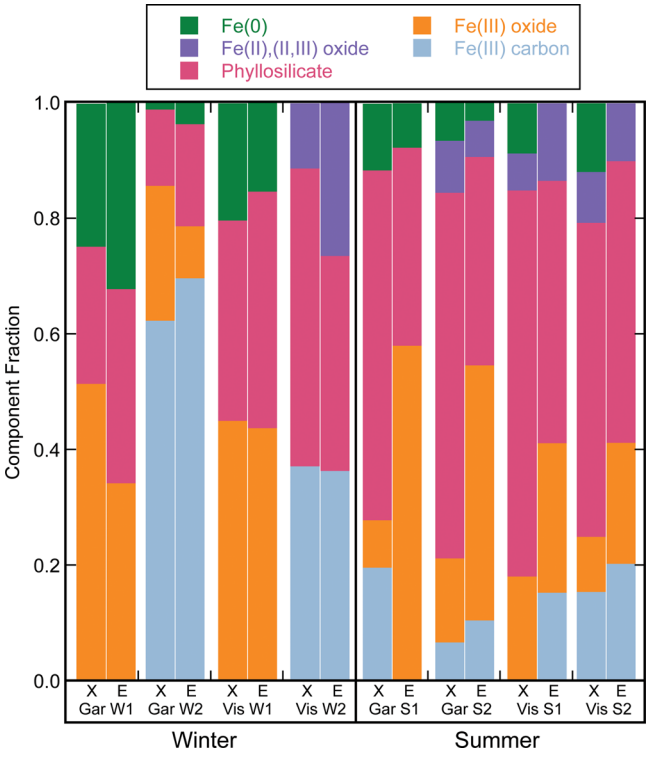


**Figure 2.** Summary of normalized component fits of Fe K-edge XAS of $PM_{2.5}$ samples for winter and summer for Fresno Garland (Gar) and Visalia (Vis). XANES (X) and EXAFS (E) parts of the spectrum were fit separately; differences in fractions determined by X and E fitting reflect differences in spectral features, background, and normalization. Details of numerical fit results are given in SI Tables S5 and S6.

For samples collected at Gar and Vis sites in January, the Fe-bearing compositional fractions were generally similar on the same collection date, but proportions of major components shifted markedly from the first week to the second. All samples contained variable fractions of phyllosilicate minerals and different types of Fe(III) oxide phases. Phyllosilicates were fit best with smectite or illite/smectite reference spectra, and Fe-rich micas (chlorite or biotite) were identified. Ferric oxide components were generally variable mixtures of ferrihydrite, goethite, hematite, and/or maghemite, which have similar but not identical spectral patterns (SI Figure S5). Between the two consecutive weeks, the estimated fraction of Fe(III) associated with organic carbon changed from no detectable fraction the first week to about 70% at Gar and 36% at Vis the following week (Figure 2), even though total $PM_{2.5}$ mass remained about the same. The Fe(III)-carbon fraction was represented by multiple reference spectra as either Fe(III) sorbed to carbon nanoparticles or Fe(III) bonded to an organic ligand in order to capture possible modes of Fe(III) bonding to carbon. Also notable in $PM_{2.5}$ samples collected the first week was a distinctive spectral signature identified as metallic iron (Fe(0)) that comprised about 32% of the normalized EXAFS spectrum at Gar and 15% at Vis. Linear combination fits of both XANES and EXAFS matched well reference spectra for either ground Fe metal and/or stainless steel, which have similar but slightly different crystal structures and thus interatomic distances (SI Figure S4). In $PM_{2.5}$ samples collected the following week, metallic Fe(0) was reduced to about 4% of the spectral signal at Gar and was not detectable at Vis, which instead contained a component of magnetite (Fe(II,III) oxide) (Figures 1 and 2). For comparison, $PM_{2.5}$ samples from Ham and Mer collected in winter (October 2011 to February 2012) were generally similar in terms of Fe-bearing component fractions to second week samples from Gar and Vis (SI Figures S10, S11, and S12). Phyllosilicate, Fe(III) oxides, and Fe(III)-organic carbon constituted the major components, whereas Fe(0) and Fe(II)/Fe(II,III) oxides were variable but consistently present as minor components.

The Fe-bearing components identified in $PM_{2.5}$ samples collected in summer (May−June) at the Gar and Vis sites one week apart were temporally more uniform than winter samples and dominated by phyllosilicate and Fe(III)-oxide phases (Figure 1, SI Figures S8 and S9). In addition to illite/smectite as the major phyllosilicate component (22−38% in EXAFS), chlorite was identified in all sample spectra (7−15%). Components representing Fe(III)-organic carbon comprised a low relative fraction (~7−20% in normalized XANES and EXAFS). Metallic Fe(0) (3−12%) and Fe(II)/Fe(II,III) oxides (6−13%) were identified as minor components in normalized XANES and EXAFS spectra from both sites on consecutive weeks (Figure 2).

*Microfocused XRF and XANES.* Microfocused ($\mu$) XRF mapping of $PM_{2.5}$ was used to locate Fe hotspots for $\mu$-XANES analysis. Because the beam spot size (~2 × 2 $\mu$m) is similar to the particle cutoff size, areas of high Fe fluorescence were generally mixtures of smaller particles. Differences among $\mu$-XANES spectra highlight the variability of Fe components in $PM_{2.5}$ but corroborate identifications from bulk spectral analysis. Similar to bulk spectra, $\mu$-XANES mostly consisted of mixtures of phyllosilicate minerals, Fe(III) oxide minerals, and Fe(III)-organic carbon in different proportions, with


https://doi.org/10.1021/acs.est.1c06962
Environ. Sci. Technol. 2022, 56, 7006−7016

different reference spectra in these classes providing the best fit (Figure 3; see SI Figure S13 for representative fit

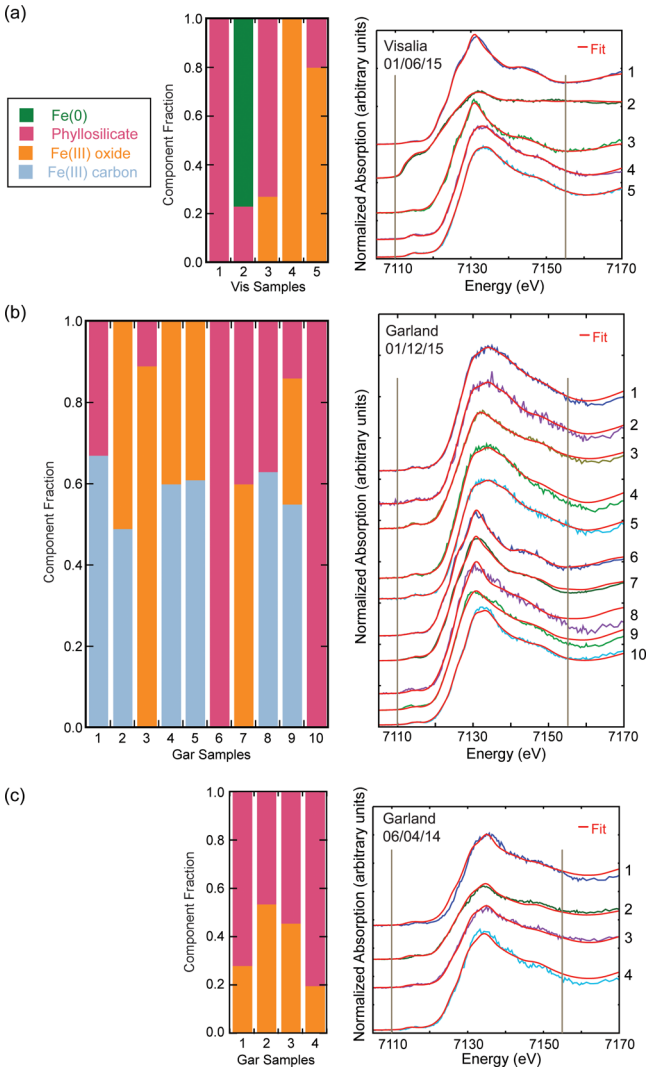


**Figure 3.** Microfocused Fe K-edge XANES fits of $PM_{2.5}$ samples: (a) Visalia (Vis) January; (b) Fresno Garland (Gar) January; (c) Gar June. Spectra were fit with two or three components, with fractions shown in bar graphs. Red lines on experimental spectra show the total best fit. Vertical gray lines show the fitted region.

deconvolutions). The phyllosilicate component was often fit with an Fe-rich reference compound such as chlorite or biotite, which was probably because high Fe minerals are more easily found in XRF mapping. Although not abundant overall, Fe(0) was found in one microfocused spectrum as a major component (Figure 3 and SI Figure S13).

**Electron Microscopy and Electron Energy-Loss Spectroscopy (EELS).** Particle morphologies from STEM provided further insight into the variability of $PM_{2.5}$, and Fe-EELS spectra enabled estimation of the average Fe oxidation state.[33] EELS analysis of multiple points on particles and aggregates showed variable $L_3/L_2$ ratios, particularly on morphological aggregrates (Figure 4). However, statistical comparisons revealed differences in average Fe oxidation state between winter and summer samples from Gar and Vis collected on the same days. Compared to reference compounds, winter particles had average $L_3/L_2$ ratios lower than summer averages, with many measurements in the $L_3/L_2$ range of Fe(0) and Fe(II) in addition to ratios representative of Fe(III) (Figure 4a). These spatially resolved results are consistent with the large fraction of Fe(0) observed in bulk X-ray absorption spectra. Summer samples by comparison had average $L_3/L_2$ ratios mostly indicative of Fe(III). For particles with ratios representative of reduced Fe, STEM images revealed irregular aggregates (~50−200 nm) consisting of acicular and blocky nanoparticles (Figure 4b). Other particles with fibrous or platy morphologies had $L_3/L_2$ ratios indicating Fe(III) (Figure 4c,d; see SI Figure S14 and S15 for additional STEM images and energy dispersive elemental spectra). Overall, the variability observed on the micro- and nano- scale was consistent with the components characterized by bulk and microfocused XAS, showing mixtures of Fe(0), Fe(II), and Fe(III) oxidation states in some particles, but a dominance of Fe(III) in the majority of particles.

## DISCUSSION

**Iron Speciation in $PM_{2.5}$.** The combination of bulk and spatially resolved methods to interrogate Fe speciation identified major Fe-bearing components and oxidation states, and provided estimates of relative spectral fractions, among the complex and variable mixtures in $PM_{2.5}$. Iron-bearing phyllosilicate minerals and Fe(III) oxides were usually the dominant fractions, but Fe(III) associated with organic carbon was also a major but variable fraction, particularly in winter. Analyses of particles at high spatial resolution by STEM and EELS confirmed that Fe(III) was the dominant oxidation state for most particles, especially in summer, consistent with results from XAS. However, STEM/EELS also showed nanoparticle aggregates with mixed Fe oxidation states of Fe(III) and Fe(II), particularly in winter samples, and confirmed the presence of metallic Fe(0) nanoparticle aggregates detected in bulk and microfocused XAS spectra. A surprising result from bulk XAS analysis was a highly variable fraction of Fe(0), as high as 32% of the Fe spectrum, estimated from LC fits in winter samples collected on the same day at Gar and Vis, and lower fractions (~0−20%) observed the following week and in summer samples.

In our prior spectromicroscopy study of $PM_{2.5}$ samples from urban Los Angeles, we discussed in detail the possible anthropogenic and geogenic sources of the major Fe-bearing species and phases.[25] We concluded that Fe-bearing particles originated mostly from combustion or abrasion emissions from anthropogenic sources, with little evidence for a large input from geogenic sources such as soils or surface deposits. In samples from the southern SJV of this study, urban centers are surrounded by agricultural lands, which should be a large source of soil-derived PM. The high fractions of phyllosilicate and Fe(III) oxide minerals prevalent in May−June $PM_{2.5}$ probably reflect larger inputs from soils during the dry summer compared to winter. Among the phases within the phyllosilicate group, however, chlorite and illite/smectite were commonly identified in spectral deconvolutions as components that were distinct from other smectite reference minerals (see Figure 1 and details in SI). While smectite-type phases are expected to dominate in oxidized soils, phyllosilicate minerals with high Fe(II) contents, such as chlorite and biotite, and other mica-type phases such as illite and vermiculite, are not typically abundant soil components. Micaceous phases are, however, a major component of brake pad and lining fillers.[36,37] Vermiculite, for example, is a common filler material


https://doi.org/10.1021/acs.est.1c06962
Environ. Sci. Technol. 2022, 56, 7006−7016

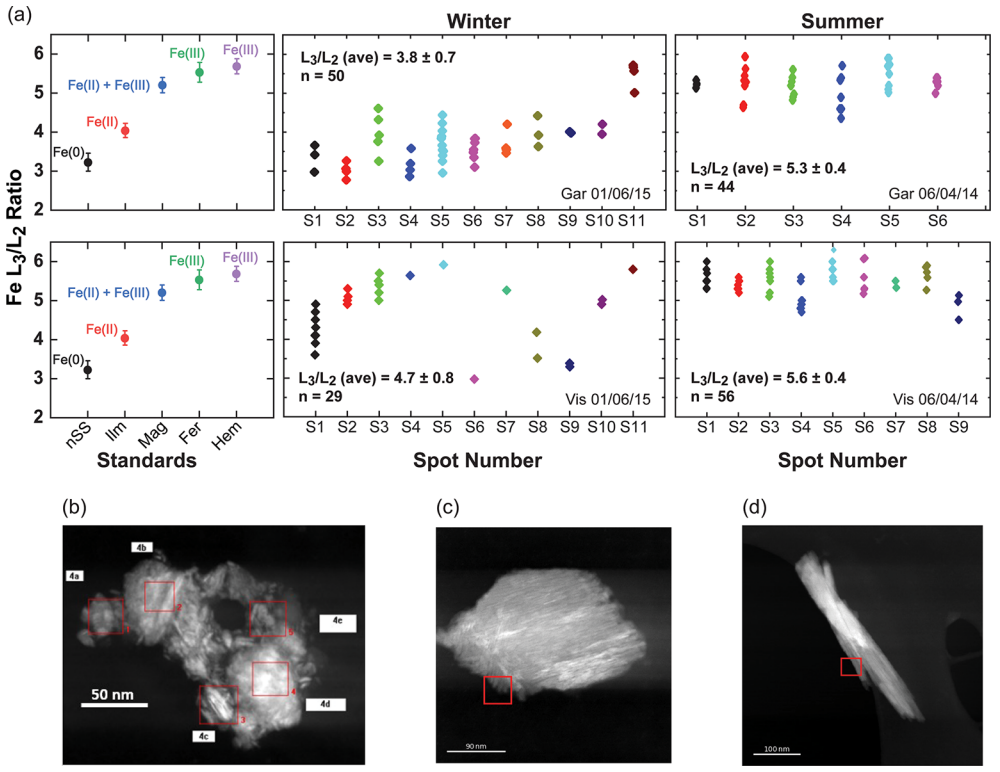


**Figure 4.** (a) Summary of electron energy loss spectroscopy (EELS) $L_3/L_2$ ratios measured on Fe-rich PM particles of winter and summer samples at Fresno Garland (Gar) and Visalia (Vis) compared with ratios of reference standards of different oxidation states. Spatial resolution was ~1−5 nm. Selected STEM images of particles measured by EELS: (b) Gar winter S4 with $L_3/L_2$ ratios indicating mostly Fe(0); (c) Gar summer S5 with Fe(III); (d) Vis summer S5 with Fe(III).

in braking systems that dehydrates to a micaceous phase during heating.[38] Thus, results suggest that the variable mixtures of phyllosilicate components identified spectroscopically probably originated from both regional agricultural soils and anthropogenic sources such vehicle brake pads and linings.

While phyllosilicates and Fe(III)-oxide phases in $PM_{2.5}$ likely reflect a mixture of anthropogenic and geogenic sources, Fe(0) and oxides with Fe(II) (primarily magnetite) are undoubtedly of anthropogenic origin. Particle aggregates with Fe(0) likely originated from either brake systems, engine wear, or other processes involving metal abrasion. Metallic Fe, together with magnetite and hematite, were reported in previous studies of PM generated by rail and subway systems and thought to originate from braking or contact between metal wheels and rails.[39,40] Magnetite nanoparticles were reported in several studies of urban PM and attributed to automobile emissions, engine wear, and brake system wear.[41,42] In $PM_{2.5}$ samples from Los Angeles, Fe(0) was a relatively small (2−6%) but easily identified component, sometimes associated with Cr, which is indicative of stainless steel.[25] Possible vehicular sources of Fe(0) are abrasion of gray cast Fe from brake rotors or brake pads containing steel fibers or Fe powders,[42,43] or engine wear of stainless steel components.[44,45] The urban centers of the SJV of this study are dissected by a major roadway and several railways, and host a variety of industries in addition to agricultural activities in the surrounding area. Thus, there is a large variety of local and regional PM sources identified by source apportionment studies with observed seasonal variations.[46,47] Road grinding, ambient weathering, and atmospheric processing of Fe(0) and Fe(II)-bearing particles will produce oxidized Fe(III) phases such as ferrihydrite (amorphous $Fe(OH)_3$), lepidocrocite ($\gamma$-FeOOH), goethite ($\alpha$-FeOOH), and sulfate-rich goethite (schwertmannite). Particle surfaces modified by emission generation processes (i.e., combustion or abrasion), and oxidized and modified by environmental weathering[42,43,48,49] would have surface chemistries reflecting alteration and mixed-metal oxidation states, and they would mix with a large and complex suite of organic compounds from combustion emissions and volatilization.[47]

**Surface Oxidation Mechanism and Generation of Biologically Damaging Species.** From a health perspective, the presence of Fe in reduced oxidation states (either Fe(0) or Fe(II)) together with Fe(III)-containing phases and reduced carbon in nanoparticle mixtures poses a significant post-inhalation risk. The combination of these reactive components may produce hydrogen peroxide ($H_2O_2$), hydroxyl radical ($\bullet OH$), hydroperoxyl radical ($HO_2\bullet$), superoxide radical ($O_2\bullet^-$), and organic radical species such as semiquinone radicals that are thought to induce inflammation and oxidative stress, and lead to pathogenesis and development of ambient particle-caused health disorders.[5,50−53] However, data on specific mechanisms and reactions associated with Fe are lacking. Here we propose possible mechanistic pathways involving Fe(0) particles and mixtures of Fe(II) and Fe(III) species, particularly as surface coatings, that may generate $H_2O_2$ and oxygen-centered radical species in post-inhalation cell exposure.

Considering nonphotolytic processes only, Figure 5 and Table 1 summarize kinetic reactions that may occur in particle-cell systems. In classic Fenton chemistry, the oxidation of Fe(II) to Fe(III) (shown in Table 1 as the species


https://doi.org/10.1021/acs.est.1c06962
Environ. Sci. Technol. 2022, 56, 7006−7016

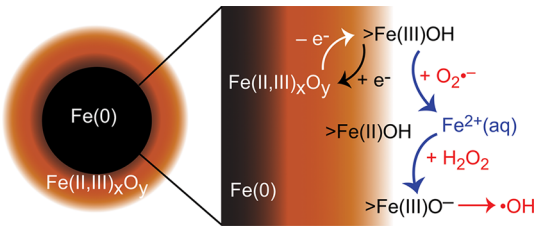


**Figure 5.** Schematic illustration of an Fe(0) particle with an Fe(II,III)-oxide surface in contact with a solution (e.g., cell fluid); blow-up shows surface functional groups denoted by > Fe(II)OH and > Fe(III)OH and possible surface reactions involving $H_2O_2$ and oxygen-centered radical species.

**Table 1. Possible Kinetic Reactions Involving Fe Particles That May Generate Oxygen and Radical Species; Reactions May Occur on Particle Surfaces or in Solution**[a]

| |
|---|
| Fe(II) Oxidation (Acidic to Neutral pH) |
| R1 $Fe(II) + H_2O_2 \rightarrow Fe(III)OH^{2+} + \bullet OH$ |
| R2 $Fe(II) + \bullet OH \rightarrow Fe(III)OH^{2+}$ |
| R3 $Fe(II) + O_2 + H_2O \rightarrow Fe(III)OH^{2+} + HO_2\bullet/(O_2\bullet^- + H^+)$ |
| R4 $Fe(II) + O_2\bullet^- + H_2O + H^+ \rightarrow Fe(III)OH^{2+} + H_2O_2$ |
| Fe(III) Reduction |
| R5 $Fe(III)OH^{2+} + H_2O_2 \rightarrow Fe(II) + H_2O/OH^- + HO_2\bullet/O_2\bullet^-$ |
| R6 $Fe(III)OH^{2+} + HO_2\bullet/O_2\bullet^- \rightarrow Fe(II) + O_2 + H_2O/OH^-$ |
| Fe(0) Oxidation |
| R7 $Fe(0) + O_2 + 2H^+ \rightarrow Fe(II) + H_2O_2$ |
| R8 $Fe(0) + H_2O_2 + 2H^+ \rightarrow Fe(II) + 2H_2O$ |
| Reactions among Oxygen Radical Species |
| R9 $H_2O_2 + \bullet OH \rightarrow HO_2\bullet + H_2O$ |
| R10 $2O_2\bullet^- + 2H^+ \rightarrow H_2O_2 + O_2$ |

[a]Compiled from Gligorovski et al.[54] and Mu et al.[59]

$Fe(III)OH^{2+}$) by $H_2O_2$ in acid solution forms •OH (R1), a strong oxidant but transient species.[54,55] Hydroxyl radical is rapidly consumed by reaction with a variety of other species, including Fe(II) (R2). Reaction intermediates such as $Fe^{IV}O^{2+}$ rather than •OH are possible at higher pH.[54,56] The oxidation of Fe(II) by $O_2$ (R3) is a relatively slow reaction that produces $HO_2\bullet$ or $O_2\bullet^-$, depending on pH, which can oxidize Fe(II) to make $H_2O_2$ (R4). In addition, Fe(III) can be reduced by $H_2O_2$ to Fe(II), with this reaction producing $HO_2\bullet/O_2\bullet^-$ (R5), which can also reduce Fe(III) to Fe(II) with formation of $O_2$ (R6). The key to continued production of radical species through the Fe redox cycle lies in maintaining a higher concentration of $H_2O_2$ than Fe(II) to prevent Fe(II) oxidation to Fe(III) from consuming •OH and $H_2O_2$ (R1, R2), and thus shutting off the reduction of Fe(III) needed to continue the cycle (R5, R6).[54]

Fenton-type reactions involving Fe(II) and Fe(III) cycling are known mostly in aqueous solution. However, zerovalent iron (ZVI) and Fe(0) nanowire studies show that they also occur at particle surfaces and in fact may be more sustainable over time because of the ability of the Fe(0) core to continue to oxidize and resupply the surface with electrons.[57−60] The surface oxidation of Fe(0) particles in air and aqueous solution has been studied extensively in the context of metal corrosion, groundwater remediation of contaminants, and many other applications. Bare Fe(0) surfaces readily and rapidly oxidize in air and oxygenated water. Depending on the setting and conditions, oxidized surface products include wustite ($Fe^{II}O$), ferrous hydroxide ($Fe^{II}(OH)_2$), magnetite, hematite, maghemite, goethite, lepidocrocite , or ferrihydrite on an Fe(0) core that may vary in thickness from a few nanometers to millimeters.[59,61−63] Figure 5 illustrates schematically how Fe(0) surface oxidation generates a mixed Fe(II,III) oxide layer in which Fe(II) or Fe(III) surface functional groups (denoted by >Fe(II)−OH and >Fe(III)−OH) may react in solution. The concentration of dissolved Fe will depend on the solubility and dissolution rate of the oxidized surface layer in contact with lung or cell fluid, which is influenced by particle size, pH, and complexing ligands.[61,63] Depending on the thickness of the oxidized layer, surface Fe(II) can be replenished by electron transfer from the interior core;[60] however, the buildup of an oxidized surface layer eventually protects the particle core from further corrosion. The oxidation of Fe(0) to Fe(II) by $O_2$ is a relatively slow reaction (R7) that produces $H_2O_2$ as an intermediate, but $H_2O_2$ can also oxidize Fe(0) (R8). The ability of Fe(0) particles to maintain a partially oxidized surface with mixtures of >Fe(II)−OH and >Fe(III)−OH functional groups that generate radical species appears to depend on surface layer thickness, rates of $H_2O_2$ production, and consumption by metals and oxygen radical species (R9, R10), and relative rates of Fe oxidation and reduction by $O_2$ and $H_2O_2$.[56,64]

Organic compounds mixed with Fe-bearing particles as observed in ambient PM may be an additional source of $H_2O_2$, $O_2\bullet^-$, and carbon-centered radical species that can react with Fe in its various forms. Electrophilic oxidized organic compounds and resonance-stabilized surface-bound radical species, known as environmentally persistent free radicals (EPFRs), have been identified in combustion products and ambient PM.[14,65−67] Quinone-type compounds (quinoids) have drawn particular interest from a health standpoint because of their ability to cycle between reduced hydroquinone, semiquinone radical, and oxidized quinone species with production of $O_2\bullet^-$ and $H_2O_2$.[53,55,68] Quinone chemistry, toxicology, and redox cycling are well-known[5,69,70] and quinoid compounds can induce antioxidant Nrf2 activation in cells.[53] A body of work on EPFRs shows that they form and are stabilized by reaction with a transition metal such as Cu or Fe.[71,72] Results from electron paramagnetic resonance (EPR) spectroscopy indicate generation of •OH and carbon-centered radical species in PM[73,74] and in model particle systems, with additional evidence for reduction of Cu or Fe.[75,76] These lines of evidence suggest multiple pathways for reaction among Fe, other redox-active metals such as Cu and possibly Mn, and reactive carbon species that can generate $H_2O_2$ and oxygen- and carbon-centered radical species.

**Implications for PM Pollution and Human Health.** Metals such as Fe that are commonly found in multiple oxidation states are believed to have a disproportionate effect in cellular response because of their ability to participate in electron transfer reactions with other metal species and organic macromolecules, thereby altering membrane and signaling functions, and promoting oxidative stress and associated inflammation.[6,51,77] In addition to directly participating in the oxidation of cellular constituents, PM activates both induction of antioxidant enzymes (Nrf2-mediated)[78,79] and increases in pro-inflammatory cytokines (NF-κB-dependent)[10,11] that are well correlated with animal exposure studies.[80] Mechanisms of biological action, however, remain


https://doi.org/10.1021/acs.est.1c06962
Environ. Sci. Technol. 2022, 56, 7006−7016

speculative and complicated by multiple pathways, which can oppose each other. An indirect pathway in which circulating cytokines generate a pro-inflammatory response to particle exposure has been proposed to explain neurological and systemic inflammation without physical translocation of particles from the respiratory system.[6,7] Conversely, nanometer-sized particles have been shown to penetrate cells, evade alveolar microphage phagocytosis, and enter the circulatory and lymphatic systems.[81] Other studies have shown inflammatory responses to Fe and Cu nanoparticle exposure in cell and animal studies, with Cu in particular demonstrating toxic effects, and suggested that differences in response are related to differences in metal solubility and particle surface reactivity.[82,83] We previously investigated the effect of silica nanoparticles with surface-adsorbed Fe on antioxidant and inflammatory responses and lipid peroxidation using human-derived THP-1 macrophages,[84,85] and showed that a delayed Nrf2 response can be activated by products of enzymes elevated through NF-κB activation.[86] Overall, however, cell and animal exposure studies using ambient PM or manufactured particles such as diesel exhaust have been inconclusive or conflicting with respect to statistical correlations between bulk chemical composition and biological response.[87,88] A recent review considers the problems that underly attempts to correlate metal content of particulates with biological effects.[89]

Our direct spectroscopic and microscopic identification of Fe in ambient $PM_{2.5}$ as a spatially and temporally variable mixture of distinct chemical species and phases, mostly present as Fe(III), but with significant fractions of metallic iron Fe(0) and Fe(II), suggests a surface chemical mechanism for generation of biologically damaging species. Reaction of cells with fine respirable particles containing mixtures of Fe and organic carbon, either on the cell surface or perhaps within the cell interior, may produce transient electron exchange reactions as described above. These reaction bursts will passivate with time as reactive species are exhausted. However, continued assault by inhaled particles over months or years may play a role in the generation of chronic pathologies that have been linked to PM exposures.

Compared to carbon-based compounds and soluble ions, Fe and other metals constitute a small fraction of PM mass. Other particle constituents in air pollution, as well as ozone, nitrogen oxides, and volatile organic compounds, contribute to the myriad of adverse health impacts and outcomes associated with poor air quality.[90,91] In general, however, the importance of metal-bearing mixtures and surface species in respirable PM in inducing adverse biological responses has not been considered in studies and is mostly unknown. The sources of particles to air emissions with metal Fe(0) and reduced Fe(II) are anthropogenic and spatially and temporally variable,[21,22,25] but expected to constitute an increasingly higher fraction on average of respirable PM in urban areas, and near roadways and transportation systems, as vehicle exhaust emissions continue to decline.[17,18] Our proposed Fenton-type reaction mechanism provides a testable system for linking the speciation of Fe and other redox-active metals to biological responses, and should be systematically investigated. These studies could help to inform atmospheric and source apportionment modeling, mechanistic toxicology, the development of sustainable nanomaterials, mitigation strategies, and regulatory policy.

## ■ ASSOCIATED CONTENT

### Supporting Information

The Supporting Information is available free of charge at https://pubs.acs.org/doi/10.1021/acs.est.1c06962.

Detailed methods on bulk chemical analyses, locations of sample sites, analysis methods for XAS data, collection methods for high resolution TEM and STEM data, analysis methods and standards for EELS data, additional XAS results for reference compounds and $PM_{2.5}$ samples, tabulated results of XAS linear combination fits, microfocused XRF and XANES, and representative STEM images and EDS results (PDF)

## ■ AUTHOR INFORMATION


### Corresponding Author

**Peggy A. O'Day** − *Life and Environmental Sciences Department and the Sierra Nevada Research Institute, University of California, Merced, California 95343, United States; Environmental Systems Graduate Program, University of California, Merced 95343, United States;* orcid.org/0000-0002-8698-5159; Email: poday@ucmerced.edu

### Authors

**Ajith Pattammattel** − *Life and Environmental Sciences Department and the Sierra Nevada Research Institute, University of California, Merced, California 95343, United States; NSLS II, Brookhaven National Laboratory, Upton, New York 11973, United States;* orcid.org/0000-0002-5956-7808

**Paul Aronstein** − *Environmental Systems Graduate Program, University of California, Merced 95343, United States*

**Valerie J. Leppert** − *Materials Science and Engineering Department, University of California, Merced, California 95343, United States*

**Henry Jay Forman** − *Life and Environmental Sciences Department and the Sierra Nevada Research Institute, University of California, Merced, California 95343, United States; Leonard Davis School of Gerontology, University of Southern California, Los Angeles, California 90089, United States*

Complete contact information is available at: https://pubs.acs.org/10.1021/acs.est.1c06962


### Notes

The authors declare no competing financial interest.

## ■ ACKNOWLEDGMENTS

This work was supported by the National Institutes of Health (grant ES023864). Use of the Stanford Synchrotron Radiation Lightsource, SLAC National Accelerator Laboratory, is supported by the U.S. Department of Energy, Office of Science, Office of Basic Energy Sciences under Contract No. DE-AC02-76SF00515. Work at the Molecular Foundry was supported by the Office of Science, Office of Basic Energy Sciences, of the U.S. Department of Energy under Contract No. DE-AC02-05CH11231. We thank the San Joaquin Valley Air Pollution Control District (SJVAPCD) for providing samples and chemical analyses, and the UC Merced Imaging and Microscopy Facility for electron microscopy support.

## REFERENCES


(1) WHO. *Ambient Air Pollution: A Global Assessment of Exposure and Burden of Disease*; World Health Organization: Geneva, Switzerland, 2016; p 131.

(2) Anderson, J. O.; Thundiyil, J. G.; Stolbach, A. Clearing the air: a review of the effects of particulate matter air pollution on human health. *J. Med. Toxicol.* **2012**, *8* (2), 166−175.

(3) USEPA *Integrated Science Assessment for Particulate Matter*; U.S. EPA: Research Triangle Park, NC, 2009; Vol. EPA/600/R-08/139F.

(4) Pope, C. A.; Lefler, J.; Ezzati, M.; Higbee, J.; Marshall, J.; Kim, S.-Y.; Bechle, M.; Gilliat, K.; Vernon, S.; Robinson, A.; Burnett, R. Mortality risk and fine particulate air pollution in a large, representative cohort of U.S. adults. *Environ. Health Persp.* **2019**, *127* (7), 077007.

(5) Yuan, X.; Miller, C. J.; Pham, A. N.; Waite, T. D. Kinetics and mechanism of auto- and copper-catalyzed oxidation of 1,4-naphthohydroquinone. *Free Rad. Bio. Med.* **2014**, *71*, 291−302.

(6) Block, M. L.; Calderon-Garciduenas, L. Air pollution: mechanisms of neuroinflammation and CNS disease. *Trends Neurosci.* **2009**, *32* (9), 506−516.

(7) Jayaraj, R. L.; Rodriguez, E. A.; Wang, Y.; Block, M. L. Outdoor ambient air pollution and neurodegenerative diseases: the neuroinflammation hypothesis. *Current Environmental Health Reports* **2017**, *4* (2), 166−179.

(8) Shaffer, R. M.; Blanco, M. N.; Li, G.; Adar, S. D.; Carone, M.; Szpiro, A. A.; Kaufman, J. D.; Larson, T. V.; Larson, E. B.; Crane, P. K.; Sheppard, L. Fine particulate matter and dementia incidence in the adult changes in thought study. *Environ. Health Persp.* **2021**, *129* (8), 087001.

(9) Li, N.; Alam, J.; Venkatesan, M. I.; Eiguren-Fernandez, A.; Schmitz, D.; Di Stefano, E.; Slaughter, N.; Killeen, E.; Wang, X.; Huang, A.; Wang, M.; Miguel, A. H.; Cho, A.; Sioutas, C.; Nel, A. E. Nrf2 is a key transcription factor that regulates antioxidant defense in macrophages and epithelial cells: protecting against the proinflammatory and oxidizing effects of diesel exhaust chemicals. *J. Immunol.* **2004**, *173* (5), 3467−3481.

(10) Becker, S.; Mundandhara, S.; Devlin, R. B.; Madden, M. Regulation of cytokine production in human alveolar macrophages and airway epithelial cells in response to ambient air pollution particles: further mechanistic studies. *Toxicol. Appl. Pharmacol.* **2005**, *207* (2 Suppl), 269−275.

(11) Baeza-Squiban, A.; Bonvallot, V.; Boland, S.; Marano, F. Airborne particles evoke an inflammatory response in human airway epithelium. activation of transcription factors. *Cell Biol. Toxicol* **1999**, *15* (6), 375−380.

(12) Carter, J. D.; Ghio, A. J.; Samet, J. M.; Devlin, R. B. Cytokine production by human airway epithelial cells after exposure to an air pollution particle is metal-dependent. *Toxicol. Appl. Pharmacol.* **1997**, *146* (2), 180−188.

(13) Valavanidis, A.; Vlachogianni, T.; Fiotakis, K.; Loridas, S. Pulmonary oxidative stress, inflammation and cancer: respirable particulate matter, fibrous dusts and ozone as major causes of lung carcinogenesis through reactive oxygen species mechanisms. *Int. J. Environ. Res. Public Health* **2013**, *10* (9).3886

(14) Li, N.; Sioutas, C.; Cho, A.; Schmitz, D.; Misra, C.; Sempf, J.; Wang, M. Y.; Oberley, T.; Froines, J.; Nel, A. Ultrafine particulate pollutants induce oxidative stress and mitochondrial damage. *Environ. Health Persp.* **2003**, *111* (4), 455−460.

(15) Knibbs, L. D.; Cole-Hunter, T.; Morawska, L. A review of commuter exposure to ultrafine particles and its health effects. *Atmos. Environ.* **2011**, *45* (16), 2611−2622.

(16) Pant, P.; Harrison, R. M. Estimation of the contribution of road traffic emissions to particulate matter concentrations from field measurements: a review. *Atmos. Environ.* **2013**, *77*, 78−97.

(17) Rexeis, M.; Hausberger, S. Trend of vehicle emission levels until 2020 - prognosis based on current vehicle measurements and future emission legislation. *Atmos. Environ.* **2009**, *43* (31), 4689−4698.

(18) Klimont, Z.; Kupiainen, K.; Heyes, C.; Purohit, P.; Cofala, J.; Rafaj, P.; Borken-Kleefeld, J.; Schopp, W. Global anthropogenic emissions of particulate matter including black carbon. *Atmos. Chem. Phys.* **2017**, *17* (14), 8681−8723.

(19) Yang, Y.; Vance, M.; Tou, F. Y.; Tiwari, A.; Liu, M.; Hochella, M. F. Nanoparticles in road dust from impervious urban surfaces: distribution, identification, and environmental implications. *Environ. Sci. Nano* **2016**, *3* (3), 534−544.

(20) Hennigan, C. J.; Mucci, A.; Reed, B. E. Trends in PM2.5 transition metals in urban areas across the United States. *Environ. Res. Lett.* **2019**, *14* (10), 10.

(21) Amato, F.; Cassee, F. R.; van der Gon, H.; Gehrig, R.; Gustafsson, M.; Hafner, W.; Harrison, R. M.; Jozwicka, M.; Kelly, F. J.; Moreno, T.; Prevot, A. S. H.; Schaap, M.; Sunyer, J.; Querol, X. Urban air quality: the challenge of traffic non-exhaust emissions. *J. Hazard. Mater.* **2014**, *275*, 31−36.

(22) Padoan, E.; Amato, F., Chapter 2 - Vehicle non-exhaust emissions: impact on air quality. In *Non-Exhaust Emissions*; Amato, F., Ed.; Academic Press, 2018; pp 21−65.

(23) Stafoggia, M.; Faustini, A., Chapter 3 - Impact on public health—epidemiological studies: a review of epidemiological studies on non-exhaust particles: identification of gaps and future needs. In *Non-Exhaust Emissions*; Amato, F., Ed.; Academic Press, 2018; pp 67−88.

(24) Khan, R. K.; Strand, M. A. Road dust and its effect on human health: a literature review. *Epidemiology and Health* **2018**, *40*, 40.

(25) Pattammattel, A.; Leppert, V. J.; Aronstein, P.; Robinson, M.; Mousavi, A.; Sioutas, C.; Forman, H. J.; O'Day, P. A. Iron speciation in particulate matter (PM2.5) from urban Los Angeles using spectromicroscopy methods. *Atmos. Environ.* **2021**, *245*, 117988.

(26) USEPA PM-2.5 (2012) Nonattainment Areas by State/County/Area. https://www3.epa.gov/airquality/greenbook/kncty.html (accessed 2021/8/31).

(27) Haley, A. D.; Broaddus, E.; Zimmerman, E.; Woolf, S. H.; Evans, B. F. *Community risk factors for mortality and exposure to environmental hazards in the San Joaquin Valley*; Virginia Commonwealth University: Richmond, VA, 2012.

(28) California Department of Public Health. California Breathing, County Asthma Data Tool. https://www.cdph.ca.gov/Programs/CCDPHP/DEODC/EHIB/CPE/Pages/CaliforniaBreathingCountyAsthmaProfiles.aspx.

(29) USEPA. *Quality Assurance Handbook for Air Pollution Measurement Systems, Vol. II: Ambient Air Quality Monitoring Program*; U.S. Environmental Protection Agency, Office of Air Quality Planning and Standards, 2013.

(30) Ravel, B.; Newville, M. ATHENA, ARTEMIS, HEPHAESTUS: Data analysis for X-ray absorption spectroscopy using IFEFFIT. *J. Synchrotron Rad.* **2005**, *12*, 537−541.

(31) O'Day, P. A.; Rivera, N.; Root, R.; Carroll, S. A. X-ray absorption spectroscopic study of iron reference compounds for the analysis of natural sediments. *Am. Mineral.* **2004**, *89* (4), 572−585.

(32) Webb, S. M. SIXpack: A graphical user interface for XAS analysis using IFEFFIT. *Phys. Scr.* **2005**, *T115*, 1011−1014.

(33) van Aken, P. A.; Liebscher, B. Quantification of ferrous/ferric ratios in minerals: new evaluation schemes of Fe L-23 electron energy-loss near-edge spectra. *Phys. Chem. Miner.* **2002**, *29* (3), 188−200.

(34) Jasinski, J.; Pinkerton, K. E.; Kennedy, I. M.; Leppert, V. J. Spatially resolved energy electron loss spectroscopy studies of iron oxide nanoparticles. *Microscopy Microanal.* **2006**, *12* (5), 424−431.

(35) Chen, K.-F.; Lo, S.-C.; Chang, L.; Egerton, R.; Kai, J.-J.; Lin, J.-J.; Chen, F.-R. Valence state map of iron oxide thin film obtained from electron spectroscopy imaging series. *Micron* **2007**, *38* (4), 354−361.

(36) Thorpe, A.; Harrison, R. M. Sources and properties of non-exhaust particulate matter from road traffic: a review. *Sci. Total Environ.* **2008**, *400* (1−3), 270−282.




https://doi.org/10.1021/acs.est.1c06962
*Environ. Sci. Technol.* 2022, 56, 7006−7016

(37) Zhao, X. G.; Ouyang, J.; Tan, Q.; Tan, X. M.; Yang, H. M. Interfacial characteristics between mineral fillers and phenolic resin in friction materials. *Mater. Exp.* **2020**, *10* (1), 70−80.
(38) Filip, P.; Weiss, Z.; Rafaja, D. On friction layer formation in polymer matrix composite materials for brake applications. *Wear* **2002**, *252* (3−4), 189−198.
(39) Eom, H. J.; Jung, H. J.; Sobanska, S.; Chung, S. G.; Son, Y. S.; Kim, J. C.; Sunwoo, Y.; Ro, C. U. Iron speciation of airborne subway particles by the combined use of energy dispersive electron probe X-ray microanalysis and Raman microspectrometry. *Anal. Chem.* **2013**, *85* (21), 10424−10431.
(40) Moreno, T.; Martins, V.; Reche, C.; Minguillón, M. C.; de Miguel, E.; Querol, X., Chapter 13 - Air quality in subway systems. In *Non-Exhaust Emissions*; Amato, F., Ed.; Academic Press, 2018; pp 289−321.
(41) Gonet, T.; Maher, B. A. Airborne, vehicle-derived Fe-bearing nanoparticles in the urban environment: a review. *Environ. Sci. Technol.* **2019**, *53* (17), 9970−9991.
(42) Kukutschová, J.; Filip, P., Chapter 6 - Review of brake wear emissions: a review of brake emission measurement studies: identification of gaps and future needs. In *Non-Exhaust Emissions*, Amato, F., Ed. Academic Press: 2018; pp 123−146.
(43) Osterle, W.; Dmitriev, A. I. The role of solid lubricants for brake friction materials. *Lubricants* **2016**, *4* (1), 22.
(44) Miller, A.; Ahlstrand, G.; Kittelson, D.; Zachariah, M. The fate of metal (Fe) during diesel combustion: morphology, chemistry, and formation pathways of nanoparticles. *Combust. Flame* **2007**, *149* (1−2), 129−143.
(45) Liati, A.; Pandurangi, S. S.; Boulouchos, K.; Schreiber, D.; Arroyo Rojas Dasilva, Y. Metal nanoparticles in diesel exhaust derived by in-cylinder melting of detached engine fragments. *Atmos. Environ.* **2015**, *101*, 34−40.
(46) Chow, J. C.; Chen, L. W. A.; Watson, J. G.; Lowenthal, D. H.; Magliano, K. A.; Turkiewicz, K.; Lehrman, D. E. PM2.5 chemical composition and spatiotemporal variability during the California Regional PM10/PM2.5 Air Quality Study (CRPAQS). *J. Geophys. Res.-Atmos.* **2006**, *111* (D10), 17.
(47) Chen, L. W. A.; Watson, J. G.; Chow, J. C.; Magliano, K. L. Quantifying PM2.5 source contributions for the San Joaquin Valley with multivariate receptor models. *Environ. Sci. Technol.* **2007**, *41* (8), 2818−2826.
(48) Shi, Z. B.; Krom, M. D.; Jickells, T. D.; Bonneville, S.; Carslaw, K. S.; Mihalopoulos, N.; Baker, A. R.; Benning, L. G. Impacts on iron solubility in the mineral dust by processes in the source region and the atmosphere: a review. *Aeolian Res.* **2012**, *5*, 21−42.
(49) Mudunkotuwa, I. A.; Pettibone, J. M.; Grassian, V. H. Environmental implications of nanoparticle aging in the processing and fate of copper-based nanomaterials. *Environ. Sci. Technol.* **2012**, *46* (13), 7001−7010.
(50) Li, N.; Xia, T.; Nel, A. E. The role of oxidative stress in ambient particulate matter-induced lung diseases and its implications in the toxicity of engineered nanoparticles. *Free Rad. Bio. Med.* **2008**, *44* (9), 1689−1699.
(51) Charrier, J. G.; McFall, A. S.; Richards-Henderson, N. K.; Anastasio, C. Hydrogen peroxide formation in a surrogate lung fluid by transition metals and quinones present in particulate matter. *Environ. Sci. Technol.* **2014**, *48* (12), 7010−7017.
(52) Tao, F.; Gonzalez-Flecha, B.; Kobzik, L. Reactive oxygen species in pulmonary inflammation by ambient particulates. *Free Rad. Bio. Med.* **2003**, *35* (4), 327−340.
(53) Xia, T.; Korge, P.; Weiss, J. N.; Li, N.; Venkatesen, M. I.; Sioutas, C.; Nel, A. Quinones and aromatic chemical compounds in particulate matter induce mitochondrial dysfunction: implications for ultrafine particle toxicity. *Environ. Health Persp.* **2004**, *112* (14), 1347−1358.
(54) Gligorovski, S.; Strekowski, R.; Barbati, S.; Vione, D. Environmental implications of hydroxyl radicals (•OH). *Chem. Rev.* **2015**, *115* (24), 13051−13092.
(55) Bolton, J. L.; Dunlap, T. Formation and biological targets of quinones: cytotoxic versus cytoprotective effects. *Chem. Res. Toxicol.* **2017**, *30* (1), 13−37.
(56) Keenan, C. R.; Sedlak, D. L. Factors affecting the yield of oxidants from the reaction of manoparticulate zero-valent iron and oxygen. *Environ. Sci. Technol.* **2008**, *42* (4), 1262−1267.
(57) Joo, S. H.; Feitz, A. J.; Sedlak, D. L.; Waite, T. D. Quantification of the oxidizing capacity of nanoparticulate zero-valent iron. *Environ. Sci. Technol.* **2005**, *39* (5), 1263−1268.
(58) Joo, S. H.; Feitz, A. J.; Waite, T. D. Oxidative degradation of the carbothioate herbicide, molinate, using nanoscale zero-valent iron. *Environ. Sci. Technol.* **2004**, *38* (7), 2242−2247.
(59) Mu, Y.; Jia, F.; Ai, Z.; Zhang, L. Iron oxide shell mediated environmental remediation properties of nano zero-valent iron. *Environmental Science: Nano* **2017**, *4* (1), 27−45.
(60) Ai, Z. H.; Gao, Z. T.; Zhang, L. Z.; He, W. W.; Yin, J. J. Core-shell structure dependent reactivity of Fe@Fe2O3 nanowires on aerobic degradation of 4-chlorophenol. *Environ. Sci. Technol.* **2013**, *47* (10), 5344−5352.
(61) He, C. S.; He, D.; Collins, R. N.; Garg, S.; Mu, Y.; Waite, T. D. Effects of Good's buffers and pH on the structural transformation of zero valent iron and the oxidative degradation of contaminants. *Environ. Sci. Technol.* **2018**, *52* (3), 1393−1403.
(62) He, D.; Ma, J. X.; Collins, R. N.; Waite, T. D. Effect of structural transformation of nanoparticulate zero-valent iron on generation of reactive oxygen species. *Environ. Sci. Technol.* **2016**, *50* (7), 3820−3828.
(63) Bae, S.; Collins, R. N.; Waite, T. D.; Hanna, K. Advances in surface passivation of nanoscale zerovalent iron: a critical review. *Environ. Sci. Technol.* **2018**, *52* (21), 12010−12025.
(64) Lee, C.; Sedlak, D. L. Enhanced formation of oxidants from bimetallic nickel-iron nanoparticles in the presence of oxygen. *Environ. Sci. Technol.* **2008**, *42* (22), 8528−8533.
(65) Dellinger, B.; Loninicki, S.; Khachatryan, L.; Maskos, Z.; Hall, R. W.; Adounkpe, J.; McFerrin, C.; Truong, H. Formation and stabilization of persistent free radicals. *Proc. Combust. Inst.* **2007**, *31*, 521−528.
(66) Valavanidis, A.; Iopoulos, N.; Gotsis, G.; Fiotakis, K. Persistent free radicals, heavy metals and PAHs generated in particulate soot emissions and residue ash from controlled combustion of common types of plastic. *J. Hazard. Mater.* **2008**, *156* (1−3), 277−284.
(67) Gehling, W.; Dellinger, B. Environmentally persistent free radicals and their lifetimes in PM2.5. *Environ. Sci. Technol.* **2013**, *47* (15), 8172−8178.
(68) Squadrito, G. L.; Cueto, R.; Dellinger, B.; Pryor, W. A. Quinoid redox cycling as a mechanism for sustained free radical generation by inhaled airborne particulate matter. *Free Rad. Bio. Med.* **2001**, *31* (9), 1132−1138.
(69) Monks, T. J.; Hanzlik, R. P.; Cohen, G. M.; Ross, D.; Graham, D. G. Quinone chemistry and toxicity. *Toxicol. Appl. Pharmacol.* **1992**, *112* (1), 2−16.
(70) O'Brien, P. J. Molecular mechanisms of quinone cytotoxicity. *Chemico-Biological Interactions* **1991**, *80* (1), 1−41.
(71) Lomnicki, S.; Truong, H.; Vejerano, E.; Dellinger, B. Copper oxide-based model of persistent free radical formation on combustion-derived particulate matter. *Environ. Sci. Technol.* **2008**, *42* (13), 4982−4988.
(72) Kiruri, L. W.; Khachatryan, L.; Dellinger, B.; Lomnicki, S. Effect of copper oxide concentration on the formation and persistency of environmentally persistent free radicals (EPFRs) in particulates. *Environ. Sci. Technol.* **2014**, *48* (4), 2212−2217.
(73) Valavanidis, A.; Fiotakis, K.; Bakeas, E.; Vlahogianni, T. Electron paramagnetic resonance study of the generation of reactive oxygen species catalysed by transition metals and quinoid redox cycling by inhalable ambient particulate matter. *Redox Report* **2005**, *10* (1), 37−51.
(74) Gehling, W.; Khachatryan, L.; Dellinger, B. Hydroxyl radical generation from environmentally persistent free radicals (EPFRs) in PM2.5. *Environ. Sci. Technol.* **2014**, *48* (8), 4266−4272.


https://doi.org/10.1021/acs.est.1c06962
*Environ. Sci. Technol.* 2022, 56, 7006−7016

(75) Nwosu, U. G.; Khachatryan, L.; Youm, S. G.; Roy, A.; dela Cruz, A. L. N.; Nesterov, E. E.; Dellinger, B.; Cook, R. L. Model system study of environmentally persistent free radicals formation in a semiconducting polymer modified copper clay system at ambient temperature. *RSC Adv.* **2016**, *6* (49), 43453−43462.
(76) Nwosu, U. G.; Roy, A.; de la Cruz, A. L. N.; Dellinger, B.; Cook, R. Formation of environmentally persistent free radical (EPFR) in iron(III) cation-exchanged smectite clay. *Environ. Sci. Process. Imp.* **2016**, *18* (1), 42−50.
(77) See, S. W.; Wang, Y. H.; Balasubramanian, R. Contrasting reactive oxygen species and transition metal concentrations in combustion aerosols. *Environ. Res.* **2007**, *103* (3), 317−324.
(78) Li, N.; Nel, A. E. Role of the Nrf2-mediated signaling pathway as a negative regulator of inflammation: implications for the impact of particulate pollutants on asthma. *Antioxid Redox Signal* **2006**, *8* (1−2), 88−98.
(79) Deng, X.; Rui, W.; Zhang, F.; Ding, W., PM induces Nrf2-mediated defense mechanisms against oxidative stress by activating PIK3/AKT signaling pathway in human lung alveolar epithelial A549 cells. *Cell Biol. Toxicol.* **2013**.*29*143
(80) Kleinman, M. T.; Araujo, J. A.; Nel, A.; Sioutas, C.; Campbell, A.; Cong, P. Q.; Li, H.; Bondy, S. C. Inhaled ultrafine particulate matter affects CNS inflammatory processes and may act via MAP kinase signaling pathways. *Toxicol. Lett.* **2008**, *178* (2), 127−130.
(81) Oberdorster, G.; Oberdorster, E.; Oberdorster, J. Nanotoxicology: an emerging discipline evolving from studies of ultrafine particles. *Environ. Health Persp.* **2005**, *113* (7), 823−839.
(82) Pettibone, J. M.; Adamcakova-Dodd, A.; Thorne, P. S.; O'Shaughnessy, P. T.; Weydert, J. A.; Grassian, V. H. Inflammatory response of mice following inhalation exposure to iron and copper nanoparticles. *Nanotoxicology* **2008**, *2* (4), 189−204.
(83) Karlsson, H. L.; Cronholm, P.; Hedberg, Y.; Tornberg, M.; De Battice, L.; Svedhem, S.; Wallirider, I. O. Cell membrane damage and protein interaction induced by copper containing nanoparticles-Importance of the metal release process. *Toxicology* **2013**, *313* (1), 59−69.
(84) Premasekharan, G.; Nguyen, K.; Contreras, J.; Ramon, V.; Leppert, V. J.; Forman, H. J. Iron-mediated lipid peroxidation and lipid raft disruption in low-dose silica-induced macrophage cytokine production. *Free Rad. Bio. Med.* **2011**, *51* (6), 1184−1194.
(85) Premshekharan, G.; Nguyen, K.; Zhang, H. Q.; Forman, H. J.; Leppert, V. J. Low dose inflammatory potential of silica particles in human-derived THP-1 macrophage cell culture studies - mechanism and effects of particle size and iron. *Chemico-Biological Interactions* **2017**, *272*, 160−171.
(86) Zhang, H.; Zhou, L.; Yuen, J.; Birkner, N.; Leppert, V.; O'Day, P. A.; Forman, H. J. Delayed Nrf2-regulated antioxidant gene induction in response to silica nanoparticles. *Free Rad. Bio. Med.* **2017**, *108*, 311−319.
(87) Zhang, H.; Haghani, A.; Mousavi, A. H.; Cacciottolo, M.; D'Agostino, C.; Safi, N.; Sowlat, M. H.; Sioutas, C.; Morgan, T. E.; Finch, C. E.; Forman, H. J. Cell-based assays that predict in vivo neurotoxicity of urban ambient nano-sized particulate matter. *Free Radic Biol. Med.* **2019**, *145*, 33−41.
(88) Weitekamp, C. A.; Kerr, L. B.; Dishaw, L.; Nichols, J.; Lein, M.; Stewart, M. J. A systematic review of the health effects associated with the inhalation of particle-filtered and whole diesel exhaust. *Inhal. Toxicol.* **2020**, *32* (1), 1−13.
(89) Forman, H. J.; Finch, C. E. A critical review of assays for hazardous components of air pollution. *Free Rad. Bio. Med.* **2018**, *117*, 202−217.
(90) Grahame, T. J.; Klemm, R.; Schlesinger, R. B. Public health and components of particulate matter: the changing assessment of black carbon. *J. Air Waste Manage. Assoc.* **2014**, *64* (6), 620−660.
(91) Manisalidis, I.; Stavropoulou, E.; Stavropoulos, A.; Bezirtzoglou, E., Environmental and health impacts of air pollution: a review. *Front. Public Health* **2020**, *8* (14). DOI: 10.3389/fpubh.2020.00014



https://doi.org/10.1021/acs.est.1c06962
*Environ. Sci. Technol.* 2022, 56, 7006−7016